THE ASTROPHYSICAL JOURNAL, 377:89–99, 1991 August 10

UNIQUE BROAD-LINE PROFILE VARIATIONS IN THE RADIO GALAXY 3C 390.3

SYLVAIN VEILLEUX
Institute for Astronomy, University of Hawaii, 2680 Woodlawn Drive, Honolulu, HI 96822
AND
WEI ZHENG
Department of Physics and Astronomy, University of Alabama, Tuscaloosa, AL 35487-0324
Received 1990 November 2; accepted 1991 February 6

ABSTRACT

We report the results of a variability study of the flux and profile of Hβ in 3C 390.3. Spectra of this object were obtained at 39 epochs during the years 1974–1988. We show that the fluctuations of the Hβ flux closely mimic the variations of the optical continuum during that period. The time scale for the emission-line variations is shorter than a year, and perhaps as short as a month. We note that the blue side of the Hβ profile ("blue bump") also followed closely the continuum variations, but the red side ("red bump") did not. The ratio of the fluxes of the blue and red bumps behaved in a very regular, nearly sinusoidal fashion. It reached a maximum in mid-1975 and at the end of 1985, a time interval of 10.4 yr. The velocity of the peak of the blueshifted bump drifted by $+900$ km s^{-1} during the 14 yr interval covered by the observations. Another emission feature at a velocity of $+4600$ km s^{-1} relative to systemic velocity was visible in the broad-line profiles of 1974–1975. Various scenarios are proposed to explain these results. The more successful models are those involving an inhomogeneous line-emitting disk or a biconical broad-line region.

Subject headings: galaxies: individual (3C 390.3) — galaxies: nuclei — galaxies: Seyfert — line profiles

1. INTRODUCTION

The most fundamental question in the study of active galactic nuclei (AGNs) is the nature of their central engine. The conventional view is that nuclear activity is caused by accretion onto a massive black hole through a disklike structure (Rees 1984). Unfortunately, the expected signatures of this accretion process are rather ambiguous. Most researchers in this field have therefore used indirect methods to study the active nucleus. The proximity of the broad-line region (BLR) and narrow-line region (NLR) to the center makes them excellent probes of the nuclear engine, and their location between the nucleus and the rest of the host galaxy suggests that they are involved in the "feeding" process. However, so little is known about the structure and dynamics of the BLR and the NLR that interpretations of the emission-line spectra in terms of the characteristics of the nucleus and the origin of the line-emitting gas are still quite speculative. Our lack of knowledge of the BLR is easy to understand: its small size ($\lesssim$0.1 pc) leaves the broad-line gas unresolved even in the closest systems. Most of our knowledge on the characteristics of the broad-line gas has been inferred from comparisons of the profiles of the spatially integrated line emission produced by different ions or by monitoring the flux and profile of the broad emission lines and comparing these results with the variations of the ultraviolet or optical continuum (e.g., Osterbrock & Mathews 1986; Blandford & McKee 1982). We will follow the second method of investigation in the present study.

Low-luminosity AGNs are generally considered better candidates for short-term monitoring because they are expected to vary on a shorter time scale than their high-luminosity counterparts [$\tau_{var} \sim$ (size of the BLR) $\sim$ (luminosity)$^{1/2}$, assuming that both the ionization parameter and the particle density are independent of the luminosity]. Among the best-studied objects are NGC 5548 (e.g., Stirpe, de Bruyn, & van Groningen 1988; Netzer et al. 1990; Peterson et al. 1990, 1991; Wamsteker et al. 1990; Clavel et al. 1991), NGC 4151 (e.g., Antonucci & Cohen 1983; Ulrich et al. 1984; Gaskell & Sparke 1986; Clavel et al. 1987), Akn 120 (e.g., Alloin, Boisson, & Pelat 1988; Peterson, Korista, & Wagner 1989), F9 (Wamsteker et al. 1985; Kollatschny & Fricke 1985; Masegosa, Moles, & Penston 1986), NGC 1566 (Alloin et al. 1985, 1986), NGC 3783 (Evans 1989), Mrk 279 (Maoz et al. 1990), Arp 102B (Miller & Peterson 1990), and 3C 390.3 (Barr et al. 1980; Yee & Oke 1981; Oke & Goodrich 1981; Peterson et al. 1984; Clavel & Wamsteker 1987; Oke 1987; Peterson, Korista, & Cota 1987; Veilleux 1988). In recent years, some efforts have been made to also monitor high-luminosity AGNs (Bregman et al. 1986; Zheng & Burbidge 1986; Zheng et al. 1987; Zheng 1988; Pérez, Penston, & Moles 1989a, b; Stockton & Farnham 1991). The results of all of these studies show that the size of the BLR of active galaxies is smaller than the value expected from photoionization models. The most promising avenues to reconcile the results of these variability studies with the predictions of photoionization models are (1) to increase the density in the BLR to (say) 10^{11} cm^{-3} (Ferland & Rees 1988; Netzer 1989) or (2) to increase the ionization parameter in the BLR (Netzer 1987, 1989; Ferland & Persson 1989) or (3) to abandon the assumption of spherical symmetry of the BLR (Bregman et al. 1986; Netzer 1987; Pérez, Penston, & Moles 1989b). This last possibility is particularly attractive in view of the growing evidence that the ionizing continuum of AGNs may be beamed along the radio axis (Browne & Murphy 1987; Unger et al. 1987; Wilson, Ward, & Haniff 1988; Pogge 1988).

The present paper reports the results of an analysis of a large set of high signal-to-noise ratio spectra of the N-galaxy 3C 390.3 obtained over the years 1974–1988. This object is a well-known double radio source with "hot spots" at the leading edge of the radio structure and a compact radio component (e.g., Harris 1972; Hargrave & McEllin 1975; Preuss et al. 1980; Dreher 1981; Laing 1981; Linfield 1981; Alef et al. 1988).

It is particularly well suited for a variability study, as it is known to vary at nearly all wavelengths (cf. references above). Moreover, the very large width of its broad emission lines (FWHM = 13,000 km s^{-1}; Osterbrock 1977) makes profile monitoring possible even at a moderate spectral resolution ($\lesssim$20 Å). In § II of this paper, we describe the data used for the analysis as well as the sources of uncertainties in the measurements. The results are presented in § 3. A number of scenarios are proposed in § 4 to explain these results. The conclusions of this study are summarized in § 5.

2. DESCRIPTION OF THE DATA SET

Over the years 1974–1984, Osterbrock, Miller, and their collaborators obtained high-quality spectra of 3C 390.3 using the image-tube image-dissector scanner system (Robinson & Wampler 1972; Miller, Robinson, & Wampler 1976; Miller, Robinson, & Schmidt 1980) with the Shane 3 m telescope of Lick Observatory. These data were taken either with a grating of 300 lines mm^{-1}, giving a resolution of approximately 20 Å, or a grating of 600 lines mm^{-1}, giving a resolution of approximately 10 Å. After 1984, spectra of 3C 390.3 were obtained using a thinned TI 800 × 800 three-phase CCD detector in conjunction with either the grism spectrograph of the UV Schmidt spectrograph on the 3 m telescope (Miller, Robinson, & Goodrich 1987). Gratings of 300 and 600 lines mm^{-1} were used, resulting in resolution of approximately 6 and 12 Å, respectively. All of these data were reduced using standard Lick Observatory programs (e.g., Osterbrock & Pogge 1985; Osterbrock & De Robertis 1985).

We decided early on to focus our attention on the Hβ profiles. This decision was made for the following reasons: (1) The temporal coverage of the Hβ data set is more complete than that of the Hα data. (2) The redshifted ($z = 0.0561$; Osterbrock, Koski, & Phillips 1975) Hα profile is strongly affected by the atmospheric B band (O_2 band near λ6850), and it is therefore very sensitive to the atmospheric correction. (3) The extreme weakness of the Mg I and Fe I absorption features at 5170–5210 Å indicates that the structure of the underlying stellar continuum does not affect significantly the profile of Hβ. In contrast, the profile of the weaker Hγ line is strongly influenced by the G band and other stellar absorption features. [O III] λ4363 emission from the active nucleus is also severely blended with Hγ. In the following discussion, the Hα and Hγ profiles will only be used for confirmation purposes.

The IDS data used here were restricted to the subset of spectra obtained with the same 2″.7 × 4″ aperture. This procedure decreases the risk of variations of the *narrow*-line fluxes introduced by extended line emission (cf. § 3), and minimizes the uncertainties on the Hβ profiles introduced by variations of the contribution of the stellar continuum to the total continuum. As in most radio galaxies, the Fe II emission in 3C 390.3 is very weak and is a negligible contaminant of Hβ (the regions affected would be $\lambda\lambda$4924 and 5018 in the rest frame of the galaxy). The principal contaminants of Hβ are [O III] $\lambda\lambda$4959, 5007 and He II λ4686. The contribution of He II to the profile of Hβ is very difficult to estimate, as its flux and profile vary in a manner which may be different from Hβ (Netzer 1982). Consequently, no attempt was made to deblend He II λ4686 from the profile of Hβ. In addition, weak sky lines at $\sim$5090 and 5180 Å can potentially affect the profle of broad Hβ. Errors introduced by the sky subtraction were minimized by excluding from the data set all of the spectra in which residuals at the position of the strong Hg 5460 Å sky line were visible. We do not believe that sky residuals affect the Hβ profiles studied here.

Table 1 lists the scans used in the present study. Listed in this table are, in order, the Julian and calendar dates of observation, the exposure time, the dispersion, the type of detector used, and the observer(s) who took the data.

3. RESULTS

The set of spectra listed in Table 1 is not homogeneous: the spectral resolution of the scans varies from 6 to 20 Å, and the flux scale is not uniform because some of the data were obtained under nonphotometric conditions. The first problem was fixed by convolving the spectra with a Gaussian with width carefully selected to produce [O III] $\lambda\lambda$4959, 5007 profiles with similar widths. Correction for the second effect was made by assuming that the flux of [O III] $\lambda\lambda$4959, 5007 was constant over the years 1974–1988. Both of these corrections were done by calculating difference spectra over the Hβ–[O III] $\lambda\lambda$4959, 5007 region. The correct scaling factor and width of the Gaussian were determined by iteration until the resulting difference spectra presented the smoothest profile at the position of [O III] $\lambda\lambda$4959, 5007. This procedure is the equivalent of scaling all of the spectra to a common [O III] flux (1.70×10^{-13} ergs s^{-1} cm^{-2}) but is considered more accurate than measuring the [O III] flux directly from the data because of the difficulty in defining the continuum level under the [O III] lines. However, a few words of caution about this fluxing procedure are needed: (1) While accurate spectrophotometry indicates that the [O III] emission lines remain constant over time scales of a few years in some galaxies (de Bruyn 1980; Oke, Readhead, & Sargent 1980; Antonucci & Cohen 1983; Peterson & Cota 1987), no studies have tested this lack of variability over a period as long as 14 years. Moreover, some of the narrow emission lines of 3C 390.3 are actually known to vary. Indeed, Clavel & Wamsteker (1987) found that the narrow core of C IV λ1549 steadily declined by a factor of 3.2 over the years 1978–1986. Barr et al. (1980) and Veilleux (1988) also reported possible flux variations of the high-ionization lines [Fe VII] λ6087 and [Fe X] λ6375 in this galaxy. On the positive side, however, photoionization models of the NLR predict that the [O III] $\lambda\lambda$4959, 5007 lines are produced at an average radius of order 10^{20} cm and are therefore not expected to vary substantially over the time interval of our study (Ferland & Osterbrock 1986, 1987). The high-ionization iron lines studied by Veilleux (1988) are produced much closer to the nucleus, and it is therefore not surprising to observe variations of these lines on a time scale of a few years. (2) This fluxing procedure also assumes that the [O III] $\lambda\lambda$4959, 5007 emitting region in 3C 390.3 is not extended over a scale larger than $\sim$2″. The data of Baum et al. (1988) make this assumption a safe one. Comparison of the present data with published photometric data will be made below to verify these assumptions. Note that, in any case, the main conclusions of the present paper relate to the *profile* variations in 3C 390.3 (e.g., relative intensity of the red and blue sides of the profile, wavelength position of the structure in the profile; cf. Figs. 2*e* and 2*f*) and are therefore independent of the scaling method used.

The spectra corrected for these two effects are presented in Figure 1. Multiple scans obtained on the same day were averaged together. The profile of broad Hβ extends over at least (-7000, $+6500$) km s^{-1} on either side of narrow Hβ (at systemic velocity) and clearly varies with time. A considerable amount of structure is usually observed in the profle of broad

TABLE 1

JOURNAL OF OBSERVATIONS

Julian Date	UT Date	Exposure (minutes)	Dispersion (Å pixel^{-1})	Detector	Observer(s)[a]
2,442,191.....	1974 May 24	32	1.25	IDS	1
2,442,227.....	1974 Jun 29	16	1.25	IDS	1
2,442,227.....	1974 Jun 29	16	1.25	IDS	1
2,442,228.....	1974 Jun 30	48	1.25	IDS	1
2,442,252.....	1974 Jul 24	64	1.25	IDS	1
2,442,567.....	1975 Jun 4	16	1.25	IDS	2
2,442,568.....	1975 Jun 5	8	1.25	IDS	2
2,442,569.....	1975 Jun 6	32	1.25	IDS	1
2,442,600.....	1975 Jul 7	16	1.25	IDS	1
2,442,600.....	1975 Jul 7	16	1.25	IDS	1
2,442,627.....	1975 Aug 3	32	1.25	IDS	1
2,442,653.....	1975 Aug 29	32	1.25	IDS	2
2,442,725.....	1975 Nov 9	32	1.25	IDS	1
2,442,866.....	1976 Mar 29	32	1.25	IDS	1
2,442,904.....	1976 May 6	32	1.25	IDS	1
2,442,948.....	1976 Jun 19	48	1.25	IDS	1
2,443,317.....	1977 Jun 23	8	1.25	IDS	2
2,444,027.....	1979 Jun 3	32	1.25	IDS	2
2,444,027.....	1979 Jun 3	32	1.25	IDS	2
2,444,027.....	1979 Jun 3	32	1.25	IDS	2
2,444,367.....	1980 May 8	32	1.25	IDS	2
2,444,378.....	1980 May 19	32	1.25	IDS	1
2,444,400.....	1980 Jun 10	32	1.25	IDS	2
2,444,430.....	1980 Jul 10	32	1.25	IDS	1
2,444,437.....	1980 Jul 17	32	2.50	IDS	2
2,444,437.....	1980 Jul 17	32	2.50	IDS	2
2,444,437.....	1980 Jul 17	32	2.50	IDS	2
2,444,467.....	1980 Aug 16	32	2.50	IDS	2
2,444,467.....	1980 Aug 16	32	2.50	IDS	2
2,444,467.....	1980 Aug 16	32	2.50	IDS	2
2,444,498.....	1980 Sep 16	32	2.50	IDS	2
2,444,521.....	1980 Oct 9	64	1.25	IDS	1
2,444,759.....	1981 Jun 4	32	2.50	IDS	2
2,444,759.....	1981 Jun 4	32	2.50	IDS	2
2,444,759.....	1981 Jun 4	32	2.50	IDS	2
2,444,791.....	1981 Jul 6	14	1.25	IDS	1
2,444,812.....	1981 Jul 27	16	1.25	IDS	1
2,445,142.....	1982 Jun 22	32	2.50	IDS	2
2,445,142.....	1982 Jun 22	32	2.50	IDS	2
2,445,142.....	1982 Jun 22	32	2.50	IDS	2
2,445,848.....	1984 May 28	16	1.25	IDS	1
2,445,848.....	1984 May 28	16	1.25	IDS	1
2,445,912.....	1984 Aug 1	30	4.00	CCD	2
2,446,262.....	1985 Jul 16	80	4.00	CCD	2
2,446,295.....	1985 Aug 18	60	2.00	CCD	2
2,446,648.....	1986 Aug 6	40	2.00	CCD	2
2,446,679.....	1986 Sep 6	40	2.00	CCD	2
2,446,741.....	1986 Nov 7	60	2.00	CCD	2
2,447,001.....	1987 Jul 25	40	2.00	CCD	2
2,447,033.....	1987 Aug 26	30	4.00	CCD	2
2,447,245.....	1988 Mar 24	50	2.00	CCD	3
2,447,367.....	1988 Jul 24	40	4.00	CCD	3

[a] Code: (1) data obtained by D. E. Osterbrock and collaborators; (2) data obtained by J. S. Miller and collaborators; (3) data obtained by S. Veilleux.

Hβ as reported in earlier studies (e.g., Lynds 1968; Burbidge & Burbidge 1971; Adams 1972; Osterbrock, Koski, & Phillips 1975). A blue "bump," extending over $v \simeq (-7000, 0)$ km s^{-1} relative to systemic velocity, is visible during the years 1974–1980 and 1985–1988. A red "bump" is also visible most of the time at $v \simeq (0, +3800)$ km s^{-1}. A third, weaker feature, partially blended with the blue wing of [O III] λ4959, is visible at $v \simeq +4600$ km s^{-1} (indicated in Fig. 1 by the vertical arrow). This feature appears to be present only in the 1974–1975 scans. This third bump is not due to [O III] emission, as it is not visible in the profile of [O III] λ5007. Its position does not correspond with any known Fe II emission line, and its

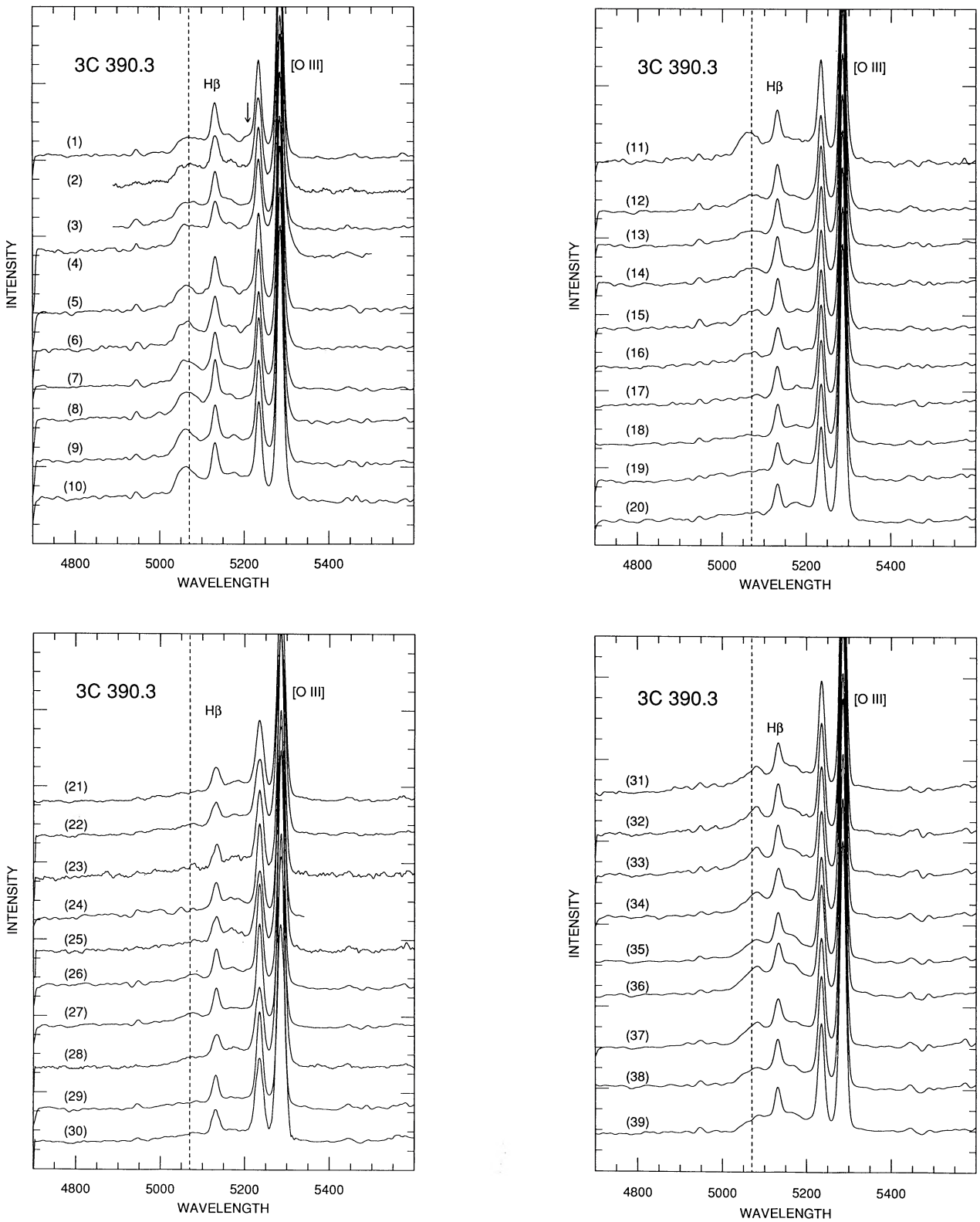

FIG. 1.—Spectra of 3C 390.3 obtained at different epochs, showing broad Hβ with superposed narrow Hβ, and [O III] $\lambda\lambda$4959, 5007. These spectra have been convolved with a Gaussian with width carefully selected to produce [O III] profiles with similar widths. They also have been scaled to a common [O III] $\lambda\lambda$4959, 5007 flux of 1.70×10^{-13} ergs s^{-1} cm^{-2}. The interval between two tick marks on the vertical axis corresponds to 5×10^{-16} ergs s^{-1} Å^{-1} cm^{-2}. For presentation purposes, each spectrum has been shifted vertically by increments of 1.0×10^{-15} ergs s^{-1} Å^{-1} cm^{-2}. The UT dates of the observations are (1) 1974 May 24, (2) 1974 June 29, (3) 1974 June 30, (4) 1974 July 24, (5) 1975 June 4, (6) 1975 June 5, (7) 1975 June 6, (8) 1975 July 7, (9) 1975 August 3, (10) 1975 August 29, (11) 1975 November 9, (12) 1976 March 29, (13) 1976 May 6, (14) 1976 June 19, (15) 1977 June 23, (16) 1979 June 3, (17) 1980 May 8, (18) 1980 May 19, (19) 1980 June 10, (20) 1980 July 10, (21) 1980 July 17, (22) 1980 August 16, (23) 1980 September 16, (24) 1980 October 9, (25) 1981 June 4, (26) 1981 July 6, (27) 1981 July 27, (28) 1982 June 22, (29) 1984 May 28, (30) 1984 August 1, (31) 1985 July 16, (32) 1985 August 18, (33) 1986 August 6, (34) 1986 September 6, (35) 1986 November 7, (36) 1987 July 25, (37) 1987 August 26, (38) 1988 March 24, (39) 1988 July 24. The vertical dashed line corresponds to the peak position of the blue bump, $\lambda = 5070$ Å, on 1974 May 24 (spectrum 1). The arrow points to a highly redshifted ($v = 4600$ km s^{-1} relative to narrow Hβ) feature in broad Hβ. This feature appears to be present only in 1974–1975.

strength does not correlate with the strength of Fe II λ5169. Further support for the reality of this Hβ feature comes from the fact that the profiles of Hα and Hγ in 1974–1975 also present a feature at that same velocity.

To investigate in a more quantitative manner the flux and profile variations of Hβ in 3C 390.3, we measured the parameters listed in Table 2. The continuum level shown in this table is the average value of the continuum level over the interval 5100–5150 Å. Measurements averaged over 5000–5320 Å gave very similar results. The Hβ fluxes, measured over 4960–5340 Å, include not only the broad and narrow components of Hβ but also a small contribution from He II λ4686. The fluxes of the blue and red bumps listed in Table 2 correspond to the Hβ fluxes over the intervals 5020–5100 Å and 5150–5200 Å, respec-

TABLE 2

RESULTS

Julian Date	F_{cont}[a]	$F_{H\beta}$[a]	F_{blue}[a]	F_{red}[a]	F_{blue}/F_{red}	λ_{blue} (Å)	λ_{red} (Å)
2,442,191.....	1.08	0.74	3.21	2.68	1.20	5070	5160:
2,442,227.....	1.21	1.24	4.97	3.87	1.29	5070	5170:
2,442,227.....	1.17	1.19	4.70	3.82	1.23	5072	5165:
2,442,228.....	1.21	1.13	4.64	3.70	1.25	5070	5160:
2,442,252.....	1.50	1.35	5.26	4.12	1.28	5070	5165:
2,442,567.....	1.09	0.78	3.87	2.78	1.39	5062	5160:
2,442,568.....	1.07	0.85	4.16	2.80	1.49	5066	5165:
2,442,569.....	1.04	0.85	4.29	2.83	1.51	5060	5160:
2,442,600.....	1.25	0.98	4.49	3.28	1.37	5063	5167:
2,442,600.....	1.15	0.95	4.49	3.17	1.42	5062	5165:
2,442,627.....	1.11	1.08	5.16	3.40	1.52	5061	5176:
2,442,653.....	1.17	0.98	4.85	3.33	1.45	5062	5177:
2,442,725.....	1.03	0.94	4.61	3.02	1.53	5065	5165:
2,442,866.....	0.72	0.61	2.84	2.01	1.41	5073	5167:
2,442,904.....	0.80	0.63	2.74	2.15	1.28	5070	5155:
2,442,948.....	0.82	0.60	2.80	2.15	1.30	5068	5160:
2,443,317.....	0.65	0.65	2.86	2.40	1.19	5075	5179:
2,444,027.....	0.65	0.48	2.26	2.36	0.96	5075	5170:
2,444,027.....	0.66	0.54	2.29	2.35	0.97	5068	5175:
2,444,027.....	0.64	0.55	2.37	2.43	0.97	5077	5172:
2,444,367.....	0.66	0.44	1.58	2.23	0.71	5081:	5178:
2,444,378.....	0.63	0.53	1.76	2.41	0.73	5060:	5175:
2,444,400.....	0.71	0.47	1.71	2.35	0.73	5075:	5171:
2,444,430.....	0.64	0.43	1.59	2.27	0.70	5081:	5176:
2,444,437.....	0.58	0.48	1.78	2.43	0.73	5070:	5181:
2,444,437.....	0.68	0.51	1.60	2.48	0.65	5060:	5180:
2,444,437.....	0.63	0.50	1.69	2.45	0.69	5060:	5182:
2,444,467.....	0.71	0.54	1.98	2.56	0.77	5079:	5172:
2,444,467.....	0.75	0.56	1.84	2.68	0.68	5073:	5175:
2,444,467.....	0.73	0.56	1.91	2.63	0.73	5075:	5174:
2,444,498.....	0.65	0.46	1.76	2.44	0.72	5077:	5178:
2,444,521.....	0.56	0.59	1.70	2.55	0.67	5062:	5175:
2,444,759.....	0.70	0.52	1.89	2.59	0.73	5080:	5169:
2,444,759.....	0.71	0.46	1.65	2.63	0.63	5081:	5169:
2,444,759.....	0.70	0.52	1.83	2.66	0.69	5080:	5169:
2,444,791.....	0.75	0.53	2.02	2.46	0.82	5079:	5170:
2,444,812.....	0.73	0.54	2.19	2.51	0.87	5077:	5172:
2,445,142.....	0.64	0.44	1.69	2.47	0.68	5080:	5175:
2,445,142.....	0.66	0.52	1.91	2.56	0.74	5070:	5163:
2,445,142.....	0.66	0.49	1.79	2.52	0.71	5070:	5172:
2,445,848.....	0.57	0.32	1.42	1.57	0.91	5086:	5168:
2,445,848.....	0.57	0.30	1.30	1.50	0.86	5085:	5168:
2,445,912.....	0.73	0.34	1.50	1.59	0.94	5082:	5171:
2,446,262.....	1.25	0.75	3.39	2.90	1.17	5080	5165:
2,446,295.....	1.20	0.76	3.63	2.91	1.25	5081	5160:
2,446,648.....	1.19	0.81	3.74	2.98	1.26	5082	5160:
2,446,679.....	1.19	0.73	3.28	2.98	1.10	5082	5160:
2,446,741.....	1.10	0.67	3.06	2.91	1.05	5080	5157:
2,447,001.....	1.28	0.92	3.98	3.51	1.13	5083	5160:
2,447,033.....	1.02	0.75	3.28	3.05	1.07	5083	5171:
2,447,245.....	1.05	0.60	2.78	2.47	1.12	5080	5163:
2,447,367.....	0.96	0.48	2.04	2.18	0.94	5087	5160:

[a] The units of F_{cont}, $F_{H\beta}$, F_{blue}, and F_{red} are 10^{-15} ergs s^{-1} cm^{-2} Å^{-1}, 10^{-13} ergs s^{-1} cm^{-2}, 10^{-14} ergs s^{-1} cm^{-2}, and 10^{-14} ergs s^{-1} cm^{-2}, respectively.

tively. The relative uncertainties on these flux measurements are $\sim \pm 10\%$, so flux variations larger than $\sim 20\%$ are probably real. The wavelength positions of the peaks of the bue and red bumps were estimated by eye. They correspond to the positions of the upper 5%–10% of the bumps. Uncertainties on the positions of the blue peak are estimated to be $\sim \pm 4$ Å. The positions of the red peak should be treated with caution, as they are considerably affected by noise. A similar warning should be given about the positions of the peak of the blue bump during the years 1980–1984, when this feature was essentially absent.

The measurements listed in Table 2 are plotted as a function of the Julian Date in Figure 2. The tendency observed in the present data for the continuum level to decrease between 1975 and 1980 (Fig. 2*a*) agrees well with the optical *B* light curve obtained by Lloyd (1984). An abrupt decrease of the continuum is observed in the present data between 1974 July 24 and 1975 June 4. The rapid brightening of the continuum at the end of 1984 was also noted by Oke (1987). Although a rigorous comparison between Lloyd's data and the present results is not possible because Lloyd's *B* light curve includes not only the continuum light but also some line emission, the variations observed in these two sets of data are of very similar amplitudes. This agreement brings some support to the validity of the assumptions used in the flux calibration. Most of the features in the light curve of the continuum emission are also seen in the light curve of the Hβ flux (Fig. 2*b*). Significant emission-line variations occur on time scales of 5 months or longer (e.g., between JD 2,442,725 and JD 2,244,866). Minor changes in the emission-line flux may be present over time scales as short as a

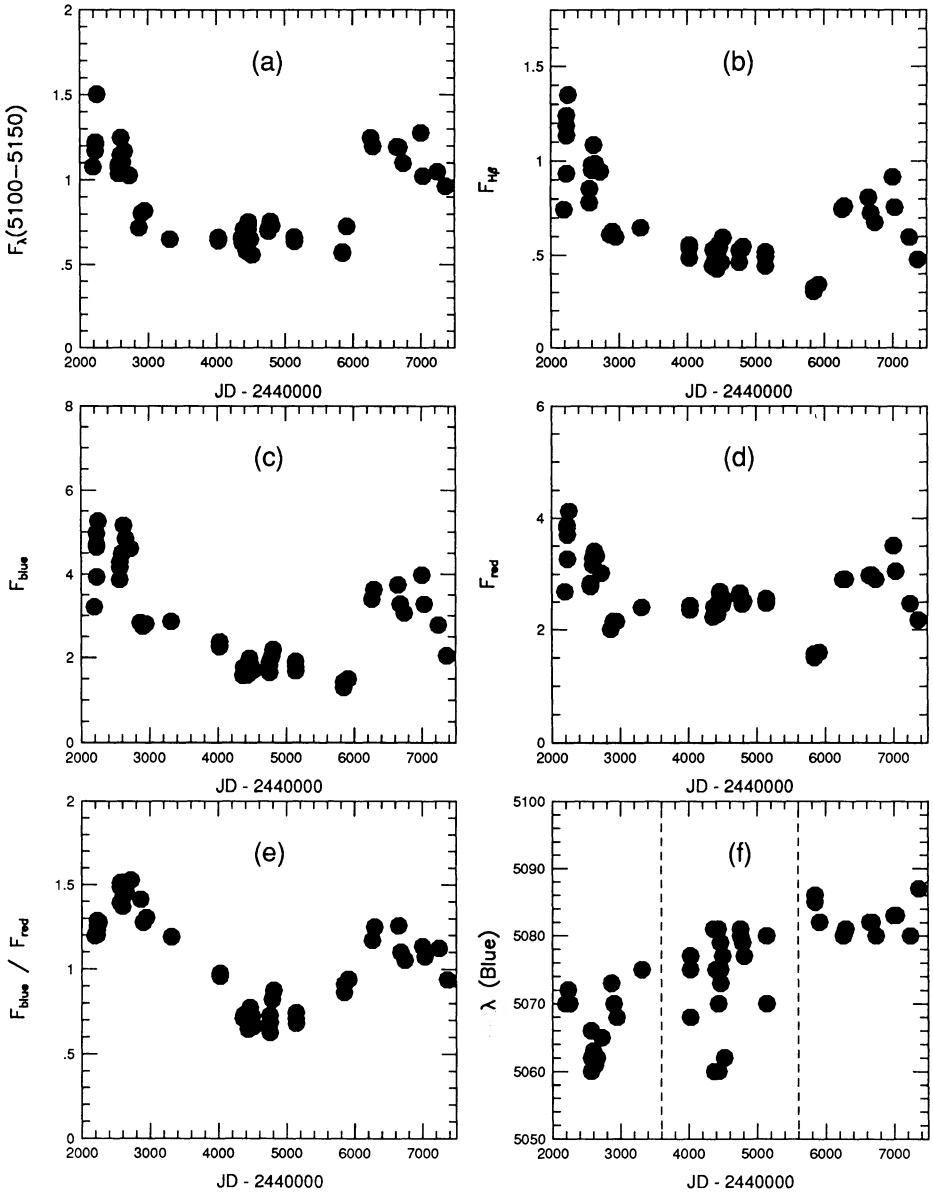

FIG. 2.—(*a*) Light curve of the continuum level measured near the position of Hβ in units of 10^{-15} ergs s^{-1} cm^{-2} Å^{-1}. (*b*) Light curve of the Hβ flux in units of 10^{-13} ergs s^{-1} cm^{-2}. (*c*) Light curve of the flux in the blue bump of Hβ in units of 10^{-14} ergs s^{-1} cm^{-2}. (*d*) Light curve of the flux in the red bump of Hβ in units of 10^{-14} ergs s^{-1} cm^{-2}. (*e*) Ratio of the fluxes of the blue and red bumps of Hβ. (*f*) Position of the peak of the blue bump of Hβ. The values of the peak positions within the vertical dashed lines are very uncertain because the blue bump was essentially absent during that period.

month (e.g., between JD 2,442,228 and JD 2,442,252, JD 2,442,567 and JD 2,442,600, and JD 2,447,001 and JD 2,447,033). A cross-correlation analysis of the Hβ flux with the continuum light-curve using the method of Edelson & Krolik (1988) does not detect any lag of the Hβ flux with respect to the continuum emission.

Figure 2*c* shows that the flux of the blue bump follows quite closely the variations of the continuum. The blue bump peaked in 1974 July and 1975 August, and then generally decreased during 1975–1984. In 1985–1986 it suddenly increased to nearly the level it had in 1974. A gradual decline of the flux of this feature was observed during 1987–1988. Again, a cross-correlation analysis does not detect any lag between the blue-bump flux and the optical continuum. The behavior of the red bump during the years 1974–1975 is similar to that of the blue bump (Fig. 2*d*). However, in contrast to the blue bump, it slowly *strengthened* during 1976–1987. The most noteworthy feature in the light curve of the red bump is the very low value it reached in 1984 May. This minimum is undoubtedly real because it is observed in two spectra obtained independently on different nights and by different observers. The red bump mimicked the behavior of the blue bump after 1987, declining gradually.

While the blue and red bumps vary in different ways, Figure 2*e* shows that the ratio of their fluxes follows a fairly smooth, nearly sinusoidal pattern. In particular, no obvious irregularity is observed between 1974 July and 1975 June or between 1984 August and 1985 July, when large changes in the continuum emission and Hβ flux are observed. The results of Oke (1987) show that the profile of Hα changed in a manner similar to the Hβ profile over the period 1981–1986. The blue-to-red flux ratio of Hβ reached a maximum at JD 2,442,600 (mid-1975) and another one at JD 2,446,400 (end of 1985), a time interval of 10.4 yr. A spectrum of 3C 390.3 obtained by H. Spinrad in 1972 (Osterbrock 1978) confirms the low value of the blue-to-red flux ratio in the early 1970s.

Finally, Figure 2*f* shows the interesting result that the wavelength of the peak of the blue bump has increased between the years 1974–1980 and 1985–1988. Its average wavelength was 5068 Å during the years 1974–1980, while it was 5082 Å during 1985–1988. Note that we cannot tell from the data whether (1) the blue bump gradually shifted from 1974 to 1988 or (2) it abruptly changed position between 1980 and 1985 or (3) the shift is due to the formation of another, less blueshifted, bump independent of the original one. A similar comparison for the red bump is not possible because the position of its peak is significantly affected by noise.

4. DISCUSSION

A natural explanation for the variations of the broad-line flux is that the BLR is responding to changes of the ionizing continuum. If all of the BLR is coherently *and* linearly responding to these changes, then the two-folding time of the broad Hβ flux, i.e., the time it takes for its intensity to increase or decrease by a factor of 2, is a measure of the light crossing time and, therefore, the size of the BLR (e.g., Gaskell & Sparke 1986; Peterson 1988). The light curve of Figure 2*b* suggests that the radius of the BLR is less than approximately 0.5 light-year. Unfortunately, a more accurate estimate of the size of the BLR cannot be derived from our results of the cross-correlation analysis of the Hβ and optical continuum light curves (§ 3). The size estimate mentioned above is in good agreement with the value determined by Clavel & Wamsteker (1987) from a cross-correlation analysis of the broad component of Lyα and C IV and the ultraviolet continuum (45 and 25 light-days, respectively).

The previous discussion is based on the crucial assumption that all of the BLR is varying coherently. This assumption is very questionable in the case of 3C 390.3. Indeed, we pointed out in § 3 that the red side of the Hβ profile is not varying in the same way as the blue side of the profile. The $v = +4600$ km s^{-1} feature noted in 1974–1975 probably represents another variable component which does not vary in phase with the other two. Consequently, the BLR of 3C 390.3 does not appear to respond as a single entity to continuum variations, and the BLR size derived by Clavel & Wamsteker (1987) and the present study should be treated with caution. A model of the structure of the BLR of 3C 390.3 is needed before we can deduce quantitative information from the light curves of Figure 2. This model must explain the following: (1) why the gas producing the blue side of Hβ is directly responding to the nuclear continuum fluctuations while the gas producing the red side is not; (2) the existence of the $v = +4600$ km s^{-1} feature and the featureless low-state profile; (3) why the position of the blue peak has changed between the years 1974–1980 and 1985–1988; (4) the smooth variations of the flux ratio of the blue and red components; and (5) the gradual increase of the flux of the red component during 1976–1987 and the deep minimum of 1984 May.

In the rest of this section, we will briefly discuss the pros and cons of various dynamical models of the BLR.

4.1. *Light Echo*

Under certain conditions, variations of the ionizing continuum can give rise to spikes/substructures in the broad-line profiles (Capriotti, Foltz, & Peterson 1982). The first condition is that the velocity field of the BLR is ordered. A variable continuum source ionizing a BLR where line broadening is caused by chaotic motion would not produce a line profile with substructure. Another condition is that the time scale of the continuum variations is of the order of the light travel time across the BLR (Peterson 1988). If these conditions are fulfilled, then one expects the displaced peaks to vary over the light travel time. This time scale is of the order of a month in 3C 390.3. Although *minor* profile variations have been detected in 3C 390.3 over an interval of the order of a month (§ 3), the position of the blue bump appears to change significantly only over a time scale much longer than the light crossing time. Light echos alone are probably not responsible for the profile substructure in 3C 390.3.

4.2. *Binary BLR*

Gaskell (1983, 1988) suggested that the double peaks and asymmetries (both blueward and redward) observed in the broad-line profiles of many active galaxies can be explained by a supermassive binary system with each binary component having its own BLR. The velocity separation of the broad-line peaks in 3C 390.3 ($\sim$6000 km s^{-1}) is consistent with the expected evolution of supermassive binaries as predicted by Begelman, Blandford, & Rees (1980). If this model indeed applies to 3C 390.3, the continuum variations shown in Figure 2*a* would be the combination of the continuum variations of each nucleus in the binary system. The strong correlation between the intensity of the blue bump and continuum emission would suggest that most of the observed optical continuum is produced by the nucleus associated with the blueshifted

BLR. The velocity drift of the blue bump would be due to changes in the apparent radial velocity of the orbiting system. If this is the case, the observed velocity shift ($\Delta v \simeq +900$ km s^{-1}) and velocity of the blue bump in 1974 ($v_{max} \simeq 4000$ km s^{-1}, assumed to be representative of the maximum radial velocity of the blueshifted BLR) imply an orbital period of $\sim 14 \times 2\pi[\cos^{-1}(1 - \Delta v/v_{max})]^{-1} = 130$ yr and an orbital radius of the blueshifted component, $a_{blue} \sim Pv_{max}/2\pi \sin i = 0.27(\sin i)^{-1}$ light-year $= 3.3(\sin i)^{-1}$ light-months (where i is the inclination of the circular orbit with respect to the plane of the sky). Following a similar argument, the orbital radius of the redshifted component is $a_{red} \simeq 1.6(\sin i)^{-1}$ light-months. Estimates of the BLR size from Clavel & Wamsteker (1987) and the present study suggest that the binary separation is barely large enough to avoid interaction between the two BLRs and produce two distinct displaced broad-line peaks as is observed. Note, however, that these size estimates are based on the assumption of a coherent BLR, which is clearly wrong in the binary picture. In this scenario, the narrow-line gas is common to both nuclei and orbits the center of mass of the system, producing a single narrow-line peak at the systemic velocity. The total mass of the system can be estimated using Kepler's third law:

$$M_{tot} = \frac{4\pi^2(a_{blue} + a_{red})^3}{GP^2}$$

$$= 1 \times 10^9 (\sin i)^{-3} M_\odot .$$

The mass of the individual components can be determined from the ratio of their apparent radial velocities relative to the systemic velocity: $M(\text{blue})/M(\text{red}) = v_{max}(\text{red})/v_{max}(\text{blue}) = 0.50$, and therefore $M(\text{blue}) = 3 \times 10^8 (\sin i)^{-3} M_\odot$ and $M(\text{red}) = 7 \times 10^8 (\sin i)^{-3} M_\odot$. These masses are considerably larger than those derived when assuming that the blueshifted and redshifted BLRs are gravitationally bound virialized systems [i.e., $M_i \simeq \sigma_i^2 R_i/G = (\text{FWHM}_i/2.354)^2 R_i/G$; $M(\text{blue}) \simeq 9 \times 10^6 M_\odot$ and $M(\text{red}) \simeq 3 \times 10^6 M_\odot$].

The binary model has problems explaining the absence of double peaks in the Hβ profiles when 3C 390.3 is in its low state. The low-state emission cannot be produced by ambient gas orbiting the center of mass of the binary because the low-state profile has a line width similar to the peak separation and its peak is redshifted by ~ 2700 km s^{-1} from the systemic velocity. The presence of the highly redshifted, $v = +4600$ km s^{-1} broad-line feature in 1974–1975 is also very difficult to explain with this model. Three-body systems are notably unstable, and one of the nuclei will be ejected through the gravitational slingshot mechanism (e.g., Saslaw, Valtonen, & Aarseth 1974). Although one may argue that this could be why the $v = +4600$ km s^{-1} component has not been observed in recent years, there is no observational evidence for ejection of pointlike sources in the core of 3C 390.3, and we therefore consider this scenario unlikely. Finally, this model cannot easily explain the regular behavior of the flux ratio of the blue and red components.

4.3. *Disk Model*

Oke (1987) suggested that the line broadening of the Balmer lines of 3C 390.3 is produced by rotating gas about the central massive source. He based his conclusion mainly on the fact that changes on the blue and red sides of Hα appeared to occur simultaneously in his data. However, his data also show that, contrary to the predictions of disk models, the blue side of the Balmer lines is not varying in the same fashion as the red side. Pérez et al. (1988) also argued in favor of an accretion disk in 3C 390.3 on the basis of the resemblance of the high-state Hβ profile with the line profile expected from a relatively simple accretion disk model. A more rigorous treatment of the relativistic effects in the accretion disk shows, however, that the profile should have a blue peak slightly higher than the red peak (Chen, Halpern, & Filippenko 1989; Chen & Halpern 1989). The resulting profiles fit the Hβ profile of Arp 102B quite well but not the Hβ profile of 3C 390.3. The third peak at $v = +4600$ km s^{-1} is also difficult to explain in this model.

A possible way out of this impasse is to have a second BLR component which does not respond in the same way and/or on the same time scale as the disk component. Such a scenario has been suggested by Alloin, Boisson, & Pelat (1988) and Stirpe, de Bruyn, & van Groningen (1988) to explain the Hα profile variations in Akn 120 and NGC 5548, respectively. In these objects, differentiation of Hα profiles obtained at different epochs results in double-peaked emission similar to the predictions of disk models. These authors proposed that the BLRs of Akn 120 and NGC 5548 are made of two distinct regions: one associated with the accretion disk and the other located well outside the disk and responding on a much longer time scale than the disk ($\gg 6$ yr in the case of Akn 120). In the case of 3C 390.3, however, subtraction of the low-state broad-line emission from the spectra obtained at different epochs cannot be explained by pure disk emission (Fig. 3). The difference profiles have irregular structure extending over approximately ± 7000

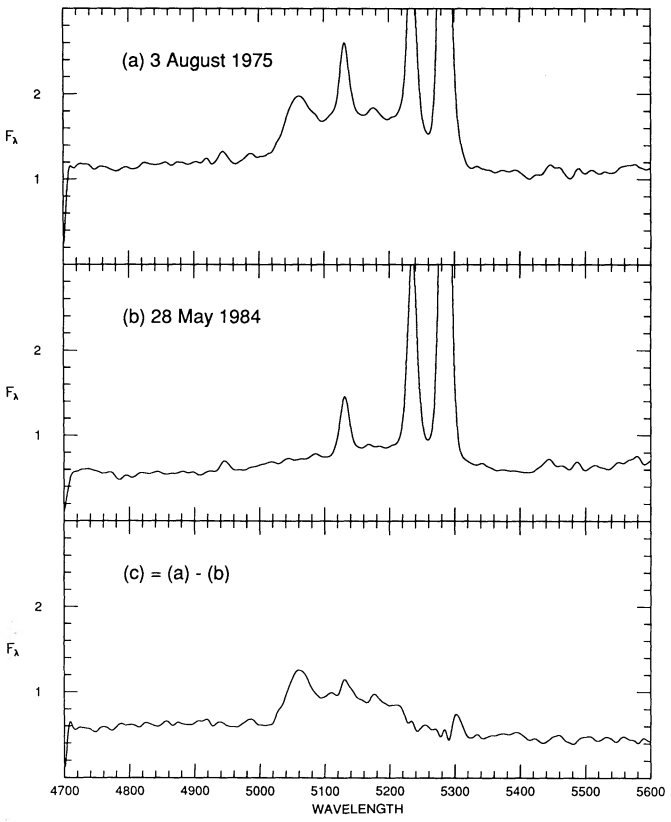

FIG. 3.—Difference spectra of broad Hβ, showing the subtraction of the low-state profile (1984 May 28) from one of the high-state profiles (1975 August 3). The resulting profile is very broad and irregular. The units of the vertical axis are 10^{-15} ergs s^{-1} cm^{-2} Å^{-1}.

km s^{-1} relative to the systemic velocity, and present multiple peaks whose relative intensities are highly variable.

The problems with the application of the disk model to 3C 390.3 can be alleviated if the disk in this object presents azimuthal asymmetries. Inhomogeneities in the disk may be responsible for some of the substructure in the profile of Hβ. These inhomogeneities would dissipate over approximately a sound crossing time

$$T_s = 40 R_S M_6 T_4^{-1/2} \text{ hr} ,$$

where R_S is the size of the disk in units of the Schwarzschild radius, M_6 is the mass of the central object in units of $10^6 M_\odot$, and T_4 is the temperature of the disk in units of 10^4 K. The mass of the central object can be estimated from the peak separation ($\sim$6000 km s^{-1}) and the approximate size of the BLR ($\sim$1 light-month; Clavel & Wamsteker 1987), $M = v^2 R/G \simeq 2 \times 10^8 M_\odot$. The size of a standard optically thick accretion disk is given by $R_S = 1250 \epsilon^{1/3} M_6^{-1/3} T_4^{-4/3}$, where ϵ is the luminosity of the disk relative to the Eddington luminosity (Pringle 1981). Using $\epsilon = 0.1$ and $T_4 = 4$, the sound crossing time $T_s \simeq 7$ yr. Inhomogeneities in the accretion disk of 3C 390.3 are therefore expected to dissipate over the time interval covered by the observations.

Nonaxisymmetric accretion of gas onto the disk may help sustain these inhomogeneities. In analogy with dwarf novae (Smak 1984), one can indeed argue that part of the emission is produced at the location where new infalling material hits the accretion disk and converts some of its kinetic energy into radiation ("hot spot"). It is tempting to associate the bumps in the emission profiles of 3C 390.3 to line-emitting gas at the hot spots. If this is the case, changes in the position of the blue peak would reflect changes in the location of one of the hot spots on the accretion disk, perhaps due to its orbital motion. Perturbations at the edge of the disk will only be felt at the center on an accretion time scale $T_a = 140 \alpha^{-1} R_s^{1/2} T_4^{-1} M_6$ yr, which is many years for the disk parameters determined earlier. Therefore, the hot spot associated with the blue bump must also produce a large fraction of the observed continuum emission to explain the fact that the strength of the blue peak follows quite closely and with a negligible time delay the intensity of the continuum. This would also explain why the red bump does not follow the continuum closely. Variations in the individual components may be due to fluctuations in their respective accretion rates. The regular behavior of the blue-to-red flux ratio may be difficult to explain in this model unless the mass accretion processes producing the blue- and redshifted hot spots are somehow related. A more complete discussion of this model is deferred until a subsequent paper (Zheng, Veilleux, & Grandi 1991).

4.4. *Double-Stream BLRs*

There is growing evidence that the ionizing radiation is not emitted isotropically from the center of AGNs. Insights into the geometry of the ionizing source can be found in the extended narrow-line region of the AGN. These regions are often observed to be elongated in the direction of the radio axis. High-ionization cones have been observed in some galaxies, suggesting that the ionizing field has a biconical geometry (Unger et al. 1987; Wilson, Ward, & Haniff 1988; Pogge 1988). Similarly, the gas in the NLR may not be distributed isotropically around the nucleus. The NLRs of Seyfert galaxies with linear radio structure are observed to be elongated along their radio axes (Whittle et al. 1988; Haniff, Wilson, & Ward 1988). A recent study suggests that the NLR is made of multiple line-emitting components, one of which is associated with the interaction of the radio plasma with the ambient gas of the host galaxy (Veilleux 1991). Whether or not the anisotropy of the ionizing radiation and/or the line-emitting gas is also present on scales as small as the BLR is not clearly established. The broad (and sometimes nearly overlapping) range of properties of the narrow-line and broad-line gas strongly suggests, however, that the transition between these two regions is not discontinuous (Wilson 1979; Osterbrock 1981; Pelat, Alloin, & Fosbury 1981; Veilleux 1988). It is therefore natural to consider BLRs with a biconical structure.

Zheng, Binette, & Sulentic (1990) found that the line profiles resulting from such "double-stream BLRs" can be similar to those produced in a spherical geometry. The profile shape depends on the radial velocity field, the projection angle, and, most important, the shell luminosity distribution in the cones. Double-peak profiles are produced when the shell luminosity distribution function peaks at a finite radius. Light travel time effects in such biconical BLRs will cause the two peaks to react differently to variations of the nuclear ionizing continuum. In the situation where the broad-line gas is outflowing from the nucleus, the blue peak is expected to be the first one to react to changes in the nuclear continuum. Such a time-lag difference between the blue and red peak responses was not detected in our rather coarsely sampled data. The shift of the position of the blue bump to larger wavelengths can be explained if the shell luminosity distribution has changed in such a way that it peaks at a radius where the gas velocity relative to the systemic velocity is smaller. Similarly, the absence of structure in the low-state profile of 3C 390.3 may be due to the fact that the shell luminosity distribution was a monotonic function with radius during that period.

The double-stream model has difficulties accounting for the third peak at $v = +4600$ km s^{-1}. Since this feature appears to have been only a transient phenomenon, it could have been caused by an inhomogeneity in the redshifted cone which simply dissipated within the time scale of a year or so. Taking this scenario one step further, it is possible that the blue and red bumps also correspond to excitation inhomogeneities or lumps entrained and confined by the biconical wind/jet. This situation has been studied theoretically by a number of researchers (e.g., Netzer 1987; Collin-Souffrin et al. 1988; Mobasher & Raine 1989). In this picture, the lump producing the blue bump is located on the near side of the nucleus, close to the ionizing source, and has a large line-of-sight velocity toward the Earth. The red bump at $v = +2000$ km s^{-1} is produced by a gas lump located on the far side of the nucleus, and far from the ionizing source, so that it responds less directly to variations of the ionizing source. The shift of the blue bump to lower velocities relative to the systemic velocity may reflect the fact that the inhomogeneity producing this feature decelerated as it moved outward from the nucleus. Variations in the blue-to-red flux ratio may be the result of light travel time effects or precession of the ionizing source.

If this scenario is correct, a lower limit to the kinematic energy involved in the motion of the blue- and redshifted lumps can be estimated from their Hβ fluxes, their apparent radial velocities, and the radio data on 3C 390.3. An estimate of the deprojected velocities of the lumps can be derived from the radio data if we assume that the blue and red components are indeed entrained in the radio plasma. Recent VLBI observa-

tions by Alef et al. (1988) have shown evidence of superluminal motion in the radio core of 3C 390.3. The superluminal velocity of the knots can be understood if relativistic beaming effects are important in the radio jet (Orr & Browne 1982; Wills & Browne 1986; Barthel 1989). Assuming a Lorentz factor, $\gamma = 5$ (Orr & Browne 1982), in the jets of 3C 390.3, the observed apparent velocity of the knots ($4.1c$ for $H_0 = 50$ km s^{-1} Mpc^{-1}) requires the source axis to lie within 22° of the line of sight. If this angle also applies to the broad-line gas, then the deprojected velocities of the blueshifted and redshifted lumps in 1974 were 4300 and 2200 km s^{-1}, respectively. During that same year, the Hβ luminosities of the blue and red bumps were $10^{41.87}$ and $10^{41.78}$ ergs s^{-1}, respectively (assuming $H_0 = 50$ km s^{-1} Mpc^{-1}), so lower limits to the masses of the blue and red bumps are $0.49(10^{10}/N_e)\ M_\odot$ and $0.40(10^{10}/N_e)\ M_\odot$, respectively. Since the bumps are not observed in any of the forbidden lines but are seen in C IV λ1549 and C III] λ1909 (Pérez et al. 1988), it is reasonable to assume that the density of the gas producing these features is $N_e \simeq 10^{9.5}$ cm^{-3}. A lower limit to the kinetic energy involved in the motion of the blue and red lumps in 1974 is therefore 4×10^{50} ergs. This corresponds to the total energy emitted by 3C 390.3 in about a day (Pérez et al. 1988).

The main argument against this jet model is of statistical nature. A number of studies have shown that Balmer line profiles with very large widths and displaced peaks are more common among radio-loud galaxies and especially in lobe-dominated sources (e.g., Setti & Woltjer 1977; Miley & Miller 1979; Bergeron & Kunth 1984; Boroson & Oke 1984; Boroson, Persson, & Oke 1985; Wills & Browne 1986). Indeed, Wills & Browne (1986) found a highly significant positive correlation between the line width of broad Hβ and the ratio of the strengths of the radio lobes and core (according to the beaming model, this ratio is largest when the radio axis is in the plane of the sky). This result is opposite to what one expects if the broad-line gas is entrained or at least moving along the radio axis, and supports instead the disk model where the broad-line gas is located in a structure perpendicular to the radio axis. The application of the biconical BLR model to 3C 390.3 will be discussed in more detail in Zheng, Veilleux, & Grandi (1991).

5. CONCLUSIONS

We studied the variability of the Hβ profiles of 3C 390.3 during the years 1974–1988. The main results of this study are the following:

1. The Hβ flux of 3C 390.3 has followed closely the variations of the optical continuum, generally decreasing during 1975–1984, before increasing rapidly in the second half of 1984 and the first half of 1985. It has been decreasing ever since (as of 1988). The time scale for significant variations is $\lesssim 0.5$ yr, with minor changes detected over a 1 month interval.

2. The Hβ profile of 3C 390.3 is characterized by two emission bumps at velocities of ~ -4000 and $+2000$ km s^{-1} relative to narrow Hβ. A third, weaker peak was detected in the profiles at $v = +4600$ km s^{-1} during 1974–1975. The flux in the main bumps did not vary in the same fashion. The blue bump closely followed the optical continuum, but the red bump did not. The most noteworthy feature in the light curve of the red bump is the gradual increase of the flux during 1976–1987 interrupted by the sudden drop in 1984 May. A year after this sharp minimum, the red bump was back to the level it had in 1982.

3. The flux ratio of the blue and red bumps varied in a very regular, almost sinusoidal fashion, peaking on $\sim$JD 2,442,600 (mid-1975) and JD 2,446,400 (end of 1985), an interval of 10.4 yr.

4. An important result of the present study is the detection of a shift of ~ 900 km s^{-1} of the blue bump during the 14 yr period covered by the observations. Unfortunately, the data do not allow us to say whether this shift has been gradual or whether it happened suddenly between 1980 and 1985.

5. A number of scenarios have been proposed to explain these results. The most successful models are those involving an inhomogeneous line-emitting disk or a biconical BLR. A more thorough investigation of these two models will be the object of a subsequent paper (Zheng, Veilleux, & Grandi 1991).

One weakness of the present investigation is the rather poor time sampling of the emission-line variations. Observations at intervals of a week or less will be needed to define accurately the shape of the light curves during these rapid variations and determine any time delay between the line fluxes and the continuum in 3C 390.3. Programs to study a few well-known Seyfert galaxies through such intense monitoring are in progress (Maoz et al. 1990; Netzer et al. 1990; Clavel et al. 1991; Peterson et al. 1991). Monitoring of 3C 390.3 over the next decade will also provide very strong constraints on the models suggested in this paper to explain the profile variations. The next logical step will be to extend the sample to other objects. Broad-line radio galaxies like 3C 390.3 are especially good targets for profile variability studies because their emission-line profiles are generally very broad and have a fair amount of structure. Simultaneous observations of numerous emission lines would be very useful in providing crucial information on the physical characteristics of the variable components(s) in the BLR.

We are very grateful to Professors Donald Osterbrock and Joseph Miller for letting us use their archive data of 3C 390.3. This project would never have been possible without their great generosity. We thank the anonymous referee for suggestions which improved this paper. S. V. would like to acknowledge the financial support of the National Science Foundation under grant NSF AST 88-18900 and the Natural Sciences and Engineering Research Council of Canada through a postdoctoral fellowship. W. Z. acknowledges the support of EPSCoR grant RII-8996152 provided jointly by NSF and the state of Alabama. CCD instrumentation and VISTA software development at Lick Observatory were funded in part by NSF Core Block grant AST 86-14519.

REFERENCES

Adams, T. F. 1972, ApJ, 172, L101
Alef, W., Götz, M. M. A., Preuss, E., & Kellermann, K. I. 1988, A&A, 192, 53
Alloin, D., Boisson, C., & Pelat, D. 1988, A&A, 200, 17
Alloin, D., Pelat, D., Phillips, M. M. Fosbury, R. A. E., & Freeman, K. 1986, ApJ, 308, 23
Alloin, D., Pelat, D., Phillips, M., & Whittle, M. 1985, ApJ, 288, 205
Antonucci, R. R. J., & Cohen, R. D. 1983, ApJ, 271, 564
Barr, P., et al. 1980, MNRAS, 193, 549
Barthel, P. D. 1989, ApJ, 336, 606
Baum, S. A., Heckman, T., Bridle, A., van Breugel, W., & Miley, G. 1988, ApJS, 68, 643
Begelman, M. C., Blandford, R. D., & Rees, M. J. 1980, Nature, 287, 307
Bergeron, J., & Kunth, D. 1984, MNRAS, 207, 263
Blandford, R. D., & McKee, C. F. 1982, ApJ, 255, 419

Boroson, T. A., & Oke, J. B. 1984, ApJ, 281, 535
Boroson, T. A., Persson, S. E., & Oke, J. B. 1985, ApJ, 293, 120
Bregman, J. N., Glassgold, A. E., Huggins, P. J., & Kinney, A. L. 1986, ApJ, 301, 698
Browne, I. W. A., & Murphy, D. W. 1987, MNRAS, 226, 101
Burbidge, E. M., & Burbidge, G. R. 1971, ApJ, 163, L21
Capriotti, E. R., Foltz, C. B., & Peterson, B. M. 1982, ApJ, 261, 35
Chen, K., & Halpern, J. P. 1989, ApJ, 344, 115
Chen, K., Halpern, J. P., & Filippenko, A. V. 1989, ApJ, 339, 742
Clavel, J., et al. 1987, ApJ, 321, 251
Clavel, J., et al. 1991, ApJ, 366, 64
Clavel, J., & Wamsteker, W. 1987, ApJ, 320, L9
Collin-Souffrin, S., Dyson, J. E., McDowell, J. C., & Perry, J. J. 1988, MNRAS, 232, 539
de Bruyn, A. G. 1980, Highlights Astr., 5, 631
Dreher, J. W. 1981, AJ, 86, 833
Edelson, R. A., & Krolik, J. H. 1988, ApJ, 331, 646
Evans, I. N. 1989, ApJ, 338, 128
Ferland, G. J., & Osterbrock, D. E. 1986, ApJ, 300, 658
———. 1987, ApJ, 318, 145
Ferland, G. J., & Persson, S. E. 1989, ApJ, 347, 656
Ferland, G. J., & Rees, M. J. 1988, ApJ, 332, 141
Gaskell, C. M. 1983, in Proc. 24th Liège Internat. Ap. Symposium, 24, 473
———. 1988, in Proc. Georgia State University Conf. on Active Galactic Nuclei, ed. H. R. Miller & P. J. Wiita (New York: Springer-Verlag), 61
Gaskell, C. M., & Sparke, L. S. 1986, ApJ, 305, 175
Haniff, C. A., Wilson, A. S., & Ward, M. J. 1988, ApJ, 334, 104
Hargrave, P. J., & McEllin, M. E. 1975, MNRAS, 173, 37
Harris, A. 1972, MNRAS, 158, 1
Kollatschny, W., & Fricke, K. J. 1985, A&A, 146, L11
Laing, R. A. 1981, MNRAS, 195, 261
Linfield, R. 1981, ApJ, 244, 436
Lloyd, C. 1984, MNRAS, 209, 697
Lynds, C. R. 1968, AJ, 73, 888
Maoz, D., et al. 1990, ApJ, 351, 75
Masegosa, J., Moles, M., & Penston, M. V. 1986, MNRAS, 218, 541
Miley, G. K., & Miller, J. S. 1979, ApJ, 228, L55
Miller, J. S., & Peterson, B. M. 1990, ApJ, 361, 98
Miller, J. S., Robinson, L. B., & Goodrich, R. W. 1987, in Instrumentation for Ground-based Optical Astronomy, ed. L. B. Robinson (New York: Springer-Verlag), 157
Miller, J. S., Robinson, L. B., & Schmidt, G. D. 1980, PASP, 92, 702
Miller, J. S., Robinson, L. B., & Wampler, E. J. 1976, Advances in Electronics and Electron Physics (New York: Academic), chap. 40B, p. 693
Mobasher, B., & Raine, D. J. 1989, MNRAS, 237, 979
Netzer, H. 1982, MNRAS, 198, 589
———. 1987, MNRAS, 225, 55
———. 1989, Comments Ap., 14, 137
Netzer, H. et al. 1990, ApJ, 353, 108
Oke, J. B. 1987, in Superluminal Radio Sources, ed. J. A. Zensus & T. J. Pearson (Cambridge: Cambridge Univ. Press), 267
Oke, J. B., & Goodrich, R. W. 1981, ApJ, 243, 445
Oke, J. B., Readhead, A. C. S., & Sargent, W. L. W. 1980, PASP, 92, 758
Orr, M. J. L., & Browne, I. W. A. 1982, MNRAS, 200, 1067
Osterbrock, D. E. 1977, ApJ, 215, 733
———. 1978, Phys. Scripta, 17, 285
———. 1981, ApJ, 246, 696
Osterbrock, D. E., & De Robertis, M. M. 1985, PASP, 97, 1129
Osterbrock, D. E., Koski, A. T., & Phillips, M. M. 1975, ApJ, 197, L41
Osterbrock, D. E., & Mathews, W. G. 1986, ARA&A, 24, 171
Osterbrock, D. E., & Pogge, R. W. 1985, ApJ, 297, 166
Pelat, D., Alloin, D., & Fosbury, R. A. E. 1981, MNRAS, 195, 787
Pérez, E., Penston, M. V., & Moles, M. 1989a, MNRAS, 239, 55
———. 1989b, MNRAS, 239, 75
Pérez, E., Penston, M. V., Tadhunter, C., Mediaville, E., & Moles, M. 1988, MNRAS, 230, 353
Peterson, B. M. 1988, PASP, 100, 18
Peterson, B. M., et al. 1991, ApJ, 368, 119
Peterson, B. M., & Cota, S. A. 1987, AJ, 94, 7
Peterson, B. M., Foltz, C. B., Crenshaw, D. M., Meyers, K. A., & Byard, P. L. 1984, ApJ, 279, 529
Peterson, B. M., Korista, K. T., & Cota, S. A. 1987, ApJ, 312, L1
Peterson, B. M., Korista, K. T., & Wagner, R. M. 1989, AJ, 98, 500
Peterson, B. M., Reichert, G. A., Korista, K. T., & Wagner, R. M. 1990, ApJ, 352, 68
Pogge, R. W. 1988, ApJ, 328, 519
Preuss, E., Kellermann, K. I., Pauliny-Toth, I. I. K., & Shaffer, D. B. 1980, ApJ, 240, L7
Pringle, J. E. 1981, ARA&A, 19, 137
Rees, M. J. 1984, ARA&A, 22, 471
Robinson, L. B., & Wampler, E. J. 1972, PASP, 84, 161
Saslaw, W. C., Valtonen, M. J., & Aarseth, S. J. 1974, ApJ, 190, 253
Setti, G., & Woltjer, L. 1977, ApJ, 218, L33
Smak, J. 1984, PASP, 96, 5
Stirpe, G. M., de Bruyn, A. G., & van Groningen, E. 1988, A&A, 200, 9
Stockton, A., & Farnham, T. 1991, ApJ, 371, 525
Ulrich, M. H., et al. 1984, MNRAS, 206, 221
Unger, S. W., Pedlar, A., Axon, D. J., Whittle, M., Meurs, E. J. A., & Ward, M. J. 1987, MNRAS, 228, 671
Veilleux, S. 1988, AJ, 95, 1695
———. 1991, ApJ, 369, 331
Wamsteker, W., Alloin, D., Pelat, D., Gilmozzi, R. 1985, ApJ, 295, L33
Wamsteker, W., et al. 1990, ApJ, 354, 446
Whittle, M., Pedlar, A., Meurs, E. J. A., Unger, S. W., Axon, D. J., and Ward, M. J. 1988, ApJ, 326, 125
Wills, B. J., & Browne, I. W. A. 1986, ApJ, 302, 56
Wilson, A. S. 1979, Proc. Roy Soc. London, A, 366, 461
Wilson, A. S., Ward, M., & Haniff, C. A. 1988, ApJ, 334, 121
Yee, H. K. C., & Oke, J. B. 1981, ApJ, 248, 472
Zheng, W. 1988, ApJ, 333, 188
Zheng, W., Binette, L., & Sulentic, J. W. 1991, ApJ, 365, 115
Zheng, W., & Burbidge, E. M. 1986, ApJ, 306, L67
Zheng, W., Burbidge, E. M., Smith, H. E., Cohen, R. D., & Bradley, S. E. 1987, ApJ, 322, 164
Zheng, W., Veilleux, S., & Grandi, S. A. 1991, ApJ, in press